

Measuring turbulence from moored acoustic Doppler velocimeters

A manual to quantifying inflow at tidal energy sites

Levi Kilcher, Jim Thomson, Joe Talbert and Alex DeKlerk

Wednesday 3rd December, 2014

Acknowledgments

The authors would like to thank Capt. Andy Reay-Ellers for his patient and precise ship-operations.

Executive Summary

This manual details a set of methods for measuring and quantifying turbulence at tidal power sites. It is written to aid site and device developers in quantifying the turbulence statistics that are important to tidal energy converter power-performance and lifetime, key parameters needed to estimate cost of energy. This manual details mooring design, instrument configuration, data processing steps and analysis guidelines for estimating turbulence statistics at tidal energy sites. This provides the tidal energy industry with a low-cost methodology for quantifying the turbulent inflow that reduces the operational lifetime of tidal energy turbines. This will help the industry to design tidal energy devices that are more reliable, less expensive and more efficient, which will lower the cost of tidal energy.

Table of Contents

1	Introduction	1
2	Measuring turbulence	2
2.1	Mooring Hardware	2
2.2	Instrument configuration	3
2.2.1	Record position and orientation of the ADV head	4
2.2.2	Software configuration	4
2.3	Deployment Planning	8
3	Data processing	8
3.1	Reading data	9
3.2	Motion Correction	9
3.2.1	Select a local coordinate system	10
3.3	Cleaning data	10
3.4	Turbulence metrics and averaging	11
3.4.1	Turbulence intensity	12
3.4.2	Turbulent kinetic energy	12
3.4.3	Reynold’s stresses	13
3.4.4	Turbulence auto-spectra	13
3.4.5	Spatial coherence	13
4	Data analysis	14
4.1	Initial inspection: time-series and histograms	14
4.2	Turbulence Spectra	14
4.3	Spatial Coherence	17
5	Summary	18
	References	21
A	Coordinate systems	23
A.1	Defining coordinate systems	23
A.2	Stationary frames	23
A.2.1	The earth frame	23
A.2.2	The analysis frame	24
A.3	Measurement frames	24
A.3.1	The ADV head	25
A.3.2	The IMU coordinate system	26
B	Filtering Acceleration	29
C	DOLfYN data processing scripts	30

List of Figures

Figure 1.	Diagram of turbulent inflow to a MHKT. The mean-flow profile is indicated in blue, and turbulent eddies of different sizes (δ), lengths (L), and orientations are indicated in red.	2
Figure 2.	Schematic diagram of the tidal turbulence mooring (TTM).	4
Figure 3.	ADV's mounted on a strongback vane prior to deployment. The heads and bodies are tilted at 15° to account for mooring blow-down. NMSS shackles and pear-links connect the strongback to the mooring lines. The strongback is leaning against the anchor stack (railroad wheels). White fair-wrap on the mooring lines is used to reduce strumming. Plastic 'zip-ties' are used to fasten the ADV cables to the vane. NMSS u-bolts and rubber gaskets fasten the ADV body to the fin. A piece of 1" angle NMSS fastened to the backbone is used to extend the ADV heads approximately 10" forward of the vane's leading edge	5
Figure 4.	The Nortek Vector program's deployment planning pane with some typical settings for quantifying turbulence at tidal-energy sites. Required settings are highlighted in red and recommended settings are in green. The blue box points out the battery consumption and memory requirement estimates for the settings shown.	7
Figure 5.	An example velocity time-series measured using a TTM at Admiralty Inlet. A) The mean streamwise velocity (\bar{u} , blue, $\Delta t = 5\text{min}$) is over-layed on the full signal (grey). B) A 5min data window of the turbulent piece of the streamwise velocity, u' . The dashed lines indicate one standard deviation.	11
Figure 6.	A time-series of turbulence statistics measured from a TTM at Admiralty Head: a) velocity, b) turbulence intensity, c) turbulent kinetic energy and its components, d) Reynold's stresses. Shaded regions indicate ebb (red) and flood (blue) periods where $U > 0.7$. Turbulence intensity is only plotted during these periods because it is meaningless for small values of U . The mean I over the data record is 10%.	15
Figure 7.	A histogram of the mean horizontal velocity magnitude.	16
Figure 8.	A comparison of the shape of spectra at two different sites from ADVs on a rigid tripod (A) and a TTM (B). The spectra for each velocity component, u , v , w are in blue, green and red, respectively. The shaded region indicates the 'inertial subrange', in which the spectra decay like $f^{-5/3}$ and all components have nearly the same amplitude. The dashed line indicates a $f^{-5/3}$ slope. The difference in amplitude of the spectra (between A and B) is expected because the turbulence measurements were made at different sites. In each panel the 'doppler noise' level arrow points at doppler noise that exceeds the high-frequency turbulence levels.	16
Figure 9.	Spectra of turbulence highlighting motion correction. A) Streamwise velocity, B) cross-stream velocity, C) vertical velocity. Black lines show the uncorrected spectra, red show spectra of head motion, and blue shows the spectra after motion correction. Green shading highlights locations where motion correction reduced the spectral amplitude. The u and v spectra have sharp peaks at 0.1Hz—and lesser peaks at higher frequencies—that match the spectrum of \bar{u}_h^e , indicating motion-contamination. Motion correction removed the vast majority of the contamination from these spectra, but contamination from the large peak in the v spectra at 0.1Hz persists. The w spectra is essentially uncontaminated by the mooring motion. The inertial sub-range is shaded as it was in Figure 8.	17
Figure 10.	Spatial coherence estimates from TTMs. Vertical coherence estimates (A) are from ADVs on TTM1 spaced 0.6m apart. Lateral coherence estimates (B) are between neighboring TTMs spaced 50m apart. Dashed lines in both figures indicate the 95% confidence level above which the coherence estimates are statistically different from 0.	18

Figure 11. The circuit-board and pressure-case end-cap of a Nortek Vector equipped with a Microstrain IMU. The ADV-body coordinate system (yellow) is depicted on the right. The notch in the end-cap defines the \hat{x}^* direction (out of the page), and the \hat{z}^* direction points back along the pressure case axis. A zoom-in on the Microstrain chip highlights its coordinate system (magenta) relative to the body. 25

Figure 12. Coordinate systems of the ADV body and head. A) A strongback with an ADV rests on a block of wood. Coordinate systems of the ADV head (magenta) and body (yellow) are shown. The \hat{x}^{head} -direction is known by the black-band around the transducer arm, and the \hat{x}^* direction is marked by a notch on the end-cap (indiscernible in the image). The cyan arrow indicates the body-to-head vector, \vec{l}_{head}^* . The perspective slightly distorts the fact that $\hat{x}^{\text{head}} \parallel -\hat{z}^*$, $\hat{y}^{\text{head}} \parallel -\hat{y}^*$, and $\hat{z}^{\text{head}} \parallel -\hat{x}^*$. B) Coordinate system of the ADV head as defined in the Nortek Vector manual (Nortek, 2005). 27

Figure 13. The ‘crop_data.pdf’ figure generated by the adv_example01.py script. The uncropped, uncleaned data is in red, and the cropped and cleaned data is in blue. 34

Figure 14. The ‘motion_vel_spec.pdf’ figure generated by the adv_example01.py script. Spikes in the spectra due to motion contamination (red) are removed by motion correction (blue). 35

1 Introduction

Turbulence is a dominant driver of the operational and extreme loads that determine hydro-kinetic turbine (HKT) lifetime. Device simulation tools, such as HydroFAST and Tidal Bladed have been developed to estimate HKT power performance and lifetimes based on device mechanical-electrical models and realistic inflow conditions. These tools help to accelerate the HKT industry by, 1) helping device designers predict failure modes in preliminary designs, and 2) providing site developers and financial institutions with estimates of the cost of energy for a particular device.

Device designers typically have all of the information necessary for producing device models for these simulations, but often lack adequate knowledge of turbulent inflow conditions to produce accurate power-performance and life-time estimates. This gap arises from the difficulty and high-cost of making turbulent inflow measurements that are relevant to HKTs. Furthermore, the method for measuring turbulent inflow must be suited to the energetic sites where HKTs will be deployed. This work aims to fill this gap by detailing a relatively low-cost and robust methodology for measuring the turbulent inflow statistics relevant to HKTs.

The question, “What turbulent statistics determine turbine device performance and fatigue loads?” motivates an active area of research in both the wind-turbine and HKT industries. While no single statistic—or group of them—has been identified that fully predicts fatigue loads, there is broad agreement that mean-shear, Reynold’s stresses, the turbulence spectrum¹, and spatial coherence all contribute significantly to fatigues loads. If turbulence is conceptualized as a mixture of eddies of different sizes, orientations and rotation speeds (Figure 1) the importance of these statistics can be understood as follows:

- Mean shear can impart a torque on the rotor shaft and induce variable loads on the blades as they rotate through the spatially non-uniform mean flow.
- The Reynold’s stresses ($\overline{u'v'}$, $\overline{u'w'}$ and $\overline{v'w'}$) indicate the orientation of the eddies in the flow. Eddies of different orientations may impart forces on different components of the turbine differently. For example an eddy aligned with the rotor ($\overline{v'w'}$ in Figure 1) will impart a large torque on the rotor that eddies of other orientations would not.
- The turbulence spectra quantifies the energy of eddies of different frequencies (from which length scales δ can be estimated). For example, an eddy with δ similar to the blade cord (l_{cord}) is likely to impart larger fatigue loads on the blade than a smaller or larger eddy with the same energy. Likewise, an eddy the same size as the rotor will impart a larger load on the rotor than a much smaller eddy. Quantifying the energy in these eddies is therefore important to accurately estimating the loads they induce.
- Spatial coherence quantifies the correlation of the turbulence in space, i.e. the length, L , of the eddies. It is important because longer eddies are likely to impart larger forces than shorter ones and longer eddies are likely to be anisotropic such that $L > \delta$.

The first two of these, mean shear and Reynold’s stresses, can be measured using acoustic Doppler profilers (ADPs) (Stacey et al., 1999; Thomson et al., 2012). The Reynold’s stresses, turbulence spectra, and spatial coherence can be measured using acoustic Doppler velocimeters (ADV). This situation requires that detailed turbulence measurements at tidal energy sites requires measurements using both ADPs and ADVs. The deployment of ADPs on the seafloor for this purpose is well described and commonly performed by engineers, scientists and ocean professionals around the world.

While ADVs have the accuracy to measure detailed statistics of turbulence, they must be positioned at a point in the flow that is relevant to HKTs, i.e. at hub-heights of 10m or more. While it is possible to do this using rigid towers, such an approach is technically challenging and expensive to implement at tidal energy sites (where currents often exceed 3 m/s). To reduce the cost of hub-height turbulence measurements this document details a methodology for making turbulence measurements from moorings. This approach is made possible by the recent integration of inertial

¹Turbulent energy and turbulence intensity can be computed from this.

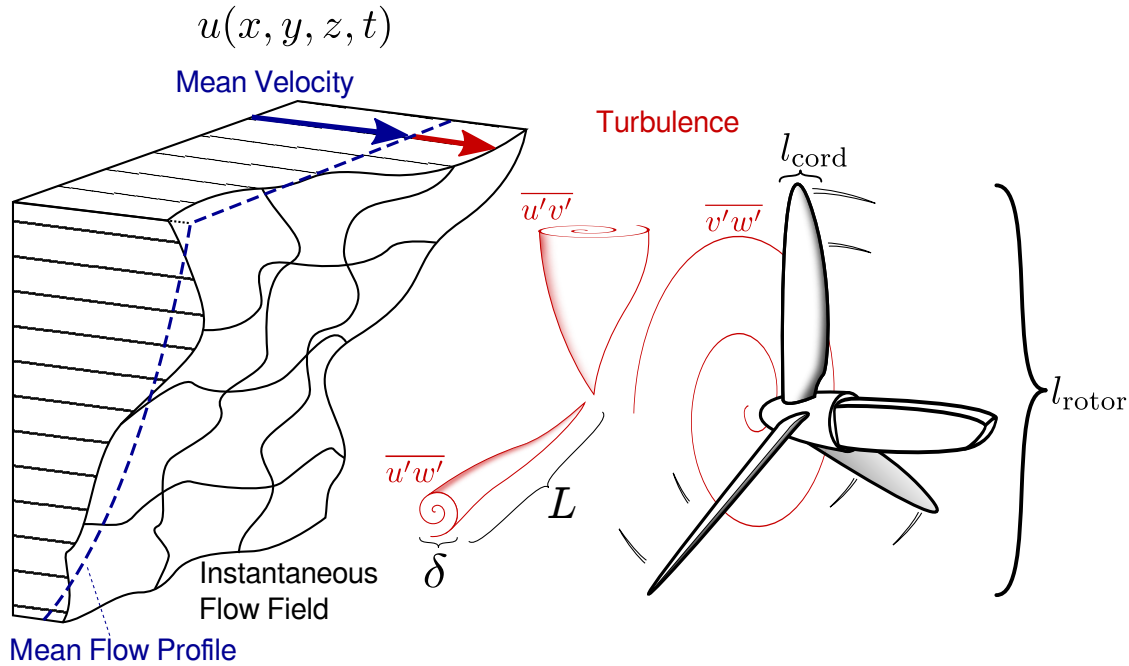


Figure 1. Diagram of turbulent inflow to a MHKT. The mean-flow profile is indicated in blue, and turbulent eddies of different sizes (δ), lengths (L), and orientations are indicated in red.

motion sensors (IMUs) into ADVs, which measuring ADV (mooring) motion so that it can be removed from the measured velocity.

Section 2 describes hardware details of the mooring used and ADV configuration details specific to moored measurements. Section 3 details the processing steps for transforming moored ADV measurements into earth-frame velocity signals and computing turbulence statistics from those measurements. Section 4 describes turbulence analysis methods that are useful to the HKT industry and defines the applicability and limitations of the results. The reader is also encouraged to download and install the Doppler Oceanography Library for pYthoN software package ([DOLFYN ikilcher.github.io/dolfyn/](https://github.com/ikilcher/dolfyn/)), which provides example instrument configuration files and functions for performing the data processing and analysis steps described herein.

2 Measuring turbulence

Acoustic Doppler velocimeters (ADV) are capable of high accuracy, precision ($< 1\%$), and sample rates (up to 64hz). These characteristics make them the preferred tool for measuring the spectrum and spatial coherence of turbulence at tidal-energy sites. However, they measure the water velocity within a few inches of the sensor-head. Therefore, in order to resolve turbulence that is relevant to MHKTs, these instruments must be positioned near the hub-height of the MHKTs that will be deployed at that location. This section describes the mooring used, and the details the configuration of instrumentation for measuring turbulence from a moored platform.

2.1 Mooring Hardware

The ‘Tidal Turbulence Mooring’ (TTM) mooring is a simple, compliant, sub-surface mooring (Thomson et al., 2013). Its primary components are a clump-weight style anchor, an acoustically triggered release for mooring recovery, mooring lines, a ‘strongback’ vane at turbine hub-height that orients the ADVs into the flow (i.e., passive

yaw), and a buoy that holds the mooring lines taught (Figure 2). The clump weight is composed of 3 railroad wheels stacked on a central steel cylinder. A steel flange welded securely to the base of the cylinder supports the weight of the wheels. The total wet-weight of the anchor is 2500lbs. Galvanized 1/2" anchor chains and a 5/8" steel shackle connect the top of the anchor-stack to the acoustic release (manufacturer: ORE, now EdgeTech). At the top of the acoustic release a high-tension swivel allows the mooring line to rotate without imparting torque on the hardware below.

The buoy for the TTM is a 37" diameter spherical steel buoy (manufacturer: McClane) that is pressure-rated for the depths to which it will be deployed. Another high-tension swivel between the buoy and mooring line allows the buoy to spin without imparting large torques on the mooring line. Half-inch Amsteel line (e.g. <http://www.amsteelblue.com/>) is used to connect the strongback-vane to the buoy and acoustic release (using 5/8" shackles). Amsteel line has a high strength-to-weight ratio, low stretch, and low torque. The half-inch line used here has a breaking strength of 30,600lbs, much larger than the dry-weight of the mooring (<3,500lbs). If modifications are made to the mooring design, to avoid catastrophic damage, be sure that the mooring line can safely support the weight of the mooring during recovery (a safety factor of at least 5× is recommended).

The 'blow-down' angle of the TTM was simulated using University of Victoria's Mooring Design and Dynamics software. The observed blow-down angle of 20° at 2m/s agreed well with the predictions (Thomson et al., 2012). This mooring design has been safely deployed in currents up to 3 m/s without exceeding a maximum advisable blow-down angle of 40°. If significant modifications are made to this mooring design (such as changes in mooring-length, deployment depth or other modifications to major hardware components), or if operating in much stronger currents, the new design should be re-simulated using a mooring simulation tool to determine blow-down angle as well as tension and drag forces.

The strongback-vane was designed to be a robust and low-cost component that effectively holds an ADV head (or two) upstream of the mooring line and holds the ADV body nearby and rigidly fixed-to its head (Figure 3). All components of the strongback-vane, including shackles, are constructed from non-magnetic materials (high-density plastics and non-magnetic stainless steel) so that the IMU-compass can accurately resolve the undistorted magnetic field of the earth (i.e. measure North). If magnetic materials must be used in the vicinity (within $\approx 2m$) of the ADV body the IMU compass should be recalibrated in the presence of those magnetic materials and in the exact orientation as they will be deployed (Nortek, 2005). At its leading edge flat-stock NMSS sandwiches the plastic-fin to form the strongback 'backbone'. 3/4" holes are drilled through the top and bottom of the backbone so that Non-Magnetic Stainless Steel (NMSS) shackles can connect the strongback to the mooring lines (Figures 3). The ADV heads and bodies are tilted 15° from the vertical-axis of the strongback to account for the 'mooring blow-down' of 10-20° at 2m/s.

2.2 Instrument configuration

When preparing instrumentation for deployment always follow the manufacturers recommendations. Be sure to:

1. Perform bench tests to confirm the instrument is operating correctly².
2. Install batteries with sufficient capacity for the deployment. Manufacturers configuration software can aid in determining battery life. It is recommended to use non-rechargeable batteries because rechargeable batteries can degrade overtime (resulting in early instrument shut-down and an incomplete data record).
3. Seal pressure-cases carefully and install dessicant (moisture-absorbing) packs to reduce the risk of water-damage to electrical hardware.
4. Synchronize instrument clocks to a single computer clock that has been recently synchronized to internet time via Network Time Protocol (NTP).
5. Configure the instrument appropriately for the deployment.

²Perform bench-tests several weeks prior to the deployment to allow time to replace faulty components if necessary.

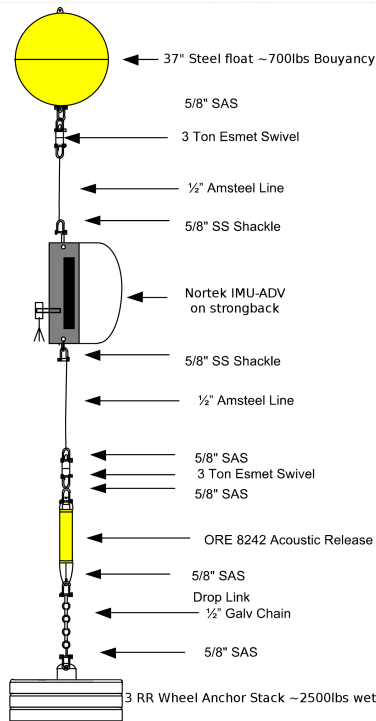


Figure 2. Schematic diagram of the tidal turbulence mooring (TTM).

In order to produce high-fidelity spectra and spatial coherence estimates from moored ADV measurements, motion-sensor measurements must be tightly synchronized with ADV velocity measurements. Currently Nortek’s VectorTM is the only instrument that can be purchased ‘off the shelf’ with a tightly synchronized inertial motion sensor (IMU). These instruments were used for the TTM test deployments.

2.2.1 Record position and orientation of the ADV head

For deployments involving cable-head IMU-ADV, it is critical to record the position and orientation of the ADV head relative to the ADV body (pressure case). Details of the definitions of these coordinate systems can be found in appendix A. The variables should be measured as accurately as possible, as errors will propagate through motion-correction calculations and lead to errors in the motion-corrected velocity measurements. As a rule of thumb: the vector \vec{l}_{head}^* should be measured to within a few mm. The orientation matrix of the ADV-head, \mathbf{H} , should be measured to within $\approx 2\%$, (≈ 2 Euler-angle degrees).

2.2.2 Software configuration

At least as important as recording the orientation of the ADV head relative to the ADV body is configuring the ADV to record the correct data channels for performing motion correction. Three primary data channels are needed to perform motion correction.

1. **The linear acceleration** vector, \vec{a} , is integrated to obtain an estimate of the translational-velocity of the ADV body and head.
2. **The angular rotation rate** vector, $\vec{\omega}$, is used to estimate the velocity of the head that is due to rotation of the ADV about the IMU.



Figure 3. ADVs mounted on a strongback vane prior to deployment. The heads and bodies are tilted at 15° to account for mooring blow-down. NMSS shackles and pear-links connect the strongback to the mooring lines. The strongback is leaning against the anchor stack (railroad wheels). White fair-wrap on the mooring lines is used to reduce strumming. Plastic 'zip-ties' are used to fasten the ADV cables to the vane. NMSS u-bolts and rubber gaskets fasten the ADV body to the fin. A piece of 1" angle NMSS fastened to the backbone is used to extend the ADV heads approximately 10" forward of the vane's leading edge

3. **The (body) orientation matrix, \mathbf{R}** , provides the orientation of the ADV body relative to the earth. It is used (with \mathbf{H}) to estimate the earth-frame orientation of the ADV-head, and thus the velocity vector in the earth-frame. It is also used to remove gravity from the linear acceleration measurement (see section 3).

The Nortek Vector can be purchased with a Microstrain GDM-GX3-25 ‘miniature attitude heading reference system’ (MicroStrain). The 3DM-GX3-25 can output all three of these channels. Sampled and stored in realtime by the same controller, the Vector velocity measurements and 3DM-GX3-25 motion and orientation measurements are tightly synchronized (to within 10^{-2} sec), allowing for high-fidelity motion-correction in post-processing. New versions of the Nortek software (bundled with a new Vector) allow the user to select which datastreams from the 3DM-GX3-25 are stored in the Vector output data file.

To set a Vector to record the correct data, open the “Vector” program and go to `Deployment » Planning » Use Existing`. For most situations you should only need to use the ‘Standard’ tab. The following settings are *required* to be able to perform motion correction (Figure 4):

1. Check the box to the left of `IMU:`.
This tells the Vector to use and record information from the IMU.
2. Select `Acc1 AngR Mag xF` from the drop-menu to the right of `IMU:`.
This tells the Vector to record the acceleration (Acc1), Angular Rate (AngR), Magnetometer (Mag), and Orientation Matrix (xF) signals³.
3. For the `Coordinate system` select `XYZ`.
This instructs the Vector to record data in the ADV-head coordinate system.

For most measurements of turbulence at tidal energy sites, the following recommendations are also likely to be appropriate:

4. Set the `Sampling Rate` to `16 Hz`.
In most tidal environments lower sampling frequencies will not resolve all of the turbulence scales. Higher sampling frequencies are typically dominated by instrument noise.
5. Set `Geography` to `Open ocean`.
This instructs the ADV to operate in ‘high’ power mode which increases data quality. Consider upgrading batteries (use 2 Lithium batteries if necessary), or using burst sampling before using lower power ‘Surf zone’ or ‘River’ setting. See the instrument manual for further details.
6. Set the `Nominal velocity range` to `+/- 4 m/s`.
Tidal velocities at most tidal energy sites will be in this range. Use the higher range of `+/- 7 m/s` if you have reason to believe the velocities will be larger than 4 m/s (at the expense of some data quality).
7. Set `Speed of Sound` to `Measured`.
The Nortek Vector uses a temperature sensor and a fixed `Salinity` value to calculate an estimate of the speed of sound (which is important to the velocity measurements). If the salinity of your site is not known consider measuring it.
8. Modify the burst interval settings to maximize data return. If you are going to the effort of putting this instrument in the water, it is valuable to capture as much turbulence data as possible. Once the above settings have been set, follow these guidelines to maximize data recovery:
 - A. Use `Continuous sampling` if possible. Consider purchasing additional batteries. With the settings recommended above, 2 Lithium batteries will last 11 days, and 2 Alkaline batteries will last 3.3 days.

³The magnetometer signal is not needed for motion correction, but the other three signals are. Note that this is the only option that provides the orientation matrix, which is required for motion correction.

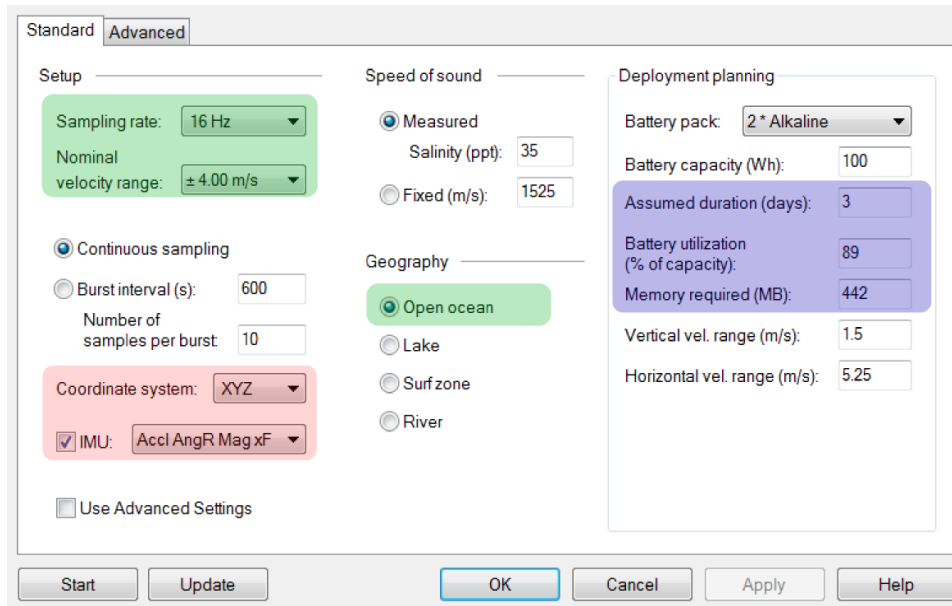


Figure 4. The Nortek Vector program's deployment planning pane with some typical settings for quantifying turbulence at tidal-energy sites. Required settings are highlighted in red and recommended settings are in green. The blue box points out the battery consumption and memory requirement estimates for the settings shown.

- B. If continuous sampling will deplete available batteries before the end of the deployment use burst sampling:
- i. Set the `Number of samples per burst` to capture 10-20min of data⁴.
 - ii. Set the `Battery pack` selection to the batteries that are available⁵.
 - iii. Adjust the burst interval—which must be greater than the sampling period—until `Battery utilization` is between 90 and 100%.
9. Be sure that the memory card in your ADV has sufficient capacity for the deployment. See the documentation for details on clearing the memory card if necessary.

For convenience, the DOLfYN software package provides a sample Nortek Vector configuration file, `Nortek_Vector_with_IMU.dep` (in the `<DOLfYN-root>/config_files/ADV/` folder) with the settings described above. To use one of these files download it, open it with the Nortek Vector software then view and adjust other parameters to fit your deployment needs as necessary⁶. The IMU-related options will be correctly pre-set when using this file.

Once you have finished setting your configuration save it to disk for later use. Before starting a deployment, make sure that your computer's system time has recently been synchronized via NTP, and that it is set to the timezone you wish the ADV data to be recorded in. If you make changes to your system time, you may need to restart your computer to make sure the new time settings propagate to the instrument.

When your system clock is updated and your configuration is ready, consider starting the deployment. If the instrument will not be deployed immediately consider using the 'delayed start' feature to reduce the risk of deploying an

⁴At 16Hz a 10min burst will have $(10 \text{ min}) \cdot (60 \text{ sec/min}) \cdot (16 \text{ samples/sec}) = 9616 \text{ samples}$.

⁵It is not recommend to use recharged Li-Ion batteries. The capacity of these batteries can be less than expected after several uses.

⁶Older versions of Nortek's Vector configuration software will not load this file correctly, be sure you have a version that supports the Microstrain chip (version 136b6 or later).

instrument that does not collect data. Take care to make sure that the start times agree with the actual physical deployment times in your cruise plan (set the instruments to start before you deploy them so that you can listen to the transmit transducer to confirm that it is operating). It is also important to synchronize your computer's clock prior to powering-down so that the clock-drift estimate provided by the Nortek Vector software is as accurate as possible.

2.3 Deployment Planning

Safe, efficient and accurate deployment of scientific equipment in the oceanic environment is a science of its own. Carefully considered planning is critical to deployment safety and success. HKT sites are generally locations of strong currents that add to the difficulty and complexity of deploying scientific equipment. It is highly recommended that deployment in these environments be led by experienced professionals in the field. At the very least, enlist such professionals to advise your planning and deployment process.

A well-written 'research cruise plan' should include the following information:

- Scientific objectives,
- A detailed schedule of all activities needed to accomplish objectives,
- Noteworthy environmental conditions at the deployment site (e.g. tidal amplitude, current amplitude, probable weather conditions, daylight hours, etc.)
- Schematic diagrams of hardware that will be deployed,
- A list of all personnel involved in the deployment,
- Maps of deployment locations that include notable bathymetric features (e.g. sub-surface ridges or canyons) and human infrastructure hazards (e.g. buoys or other equipment).
- A risk assessment and risk mitigation plan.

The schedule is one of the most important parts of the cruise plan. It should include personnel arrival/departure times, ship arrival/departure times, ship-loading and ship-preparation periods, transit periods between port and deployment locations, and target deployment times. Deployment and recovery should be conducted during slack tides to minimize risks associated with the strong currents present during ebb and flood. When preparing the schedule take care to realistically assess the time needed for each piece of the cruise; when in doubt allow 'contingency' time for each period. The instruments should be deployed for at least two full-tidal cycles, and ideally up-to 6 or more tidal cycles. Site characterization measurements for power availability should be much longer (see Polagye and Thomson, 2013).

3 Data processing

Data processing involves reading raw data from an instrument and converting it to a form that can be readily analyzed, in general it includes cleaning (removing) 'bad' data points, converting to consistent scientific units, producing high- or mid-level variables from the raw data and averaging.

Often times during the analysis stage unexpected or unrealistic results will indicate errors in the data. When this happens it is necessary to cycle back through data processing steps to inspect raw data and locate the source of the error and clean (remove) bad data. The difference between good and bad data is generally stark, but when it is not and no viable justification can be made for removing the unexpected data one should err on the side of keeping the data and, if necessary, treating it as a special case.

Fortunately, the reliability of velocity measurements from instruments such as ADVs and ADPs is high, the uncertainties well understood and methods for cleaning data are well defined. Instruments generally provide estimates of various sources of uncertainty and other errors as part of their output data streams (e.g. 'error velocity' and beam 'correlation') that aid in cleaning data.

As the scientific community has become familiar with these measurements, well defined and justified methods for cleaning data have been developed and shown to be effective (e.g. Goring and Nikora, 2002). This means that it is now possible to generate meaningful and reliable statistics with minimal user input and inspection. The DOLfYN software package includes tools and scripts for processing and analyzing turbulence measurements made following the procedures in this document.

There are four major steps to processing moored ADV data:

1. read the raw data from the ADV data file and crop it to the period of interest,
2. remove ADV head-motion from measured velocity and rotate data into a useful coordinate system,
3. clean erroneous points from the ADV data record,
4. compute turbulence statistics and averages.

It is common practice to save the results of these steps some or all of these steps so that later analysis does not require reprocessing (which sometimes requires significant CPU-time). The DOLfYN software package has tools for performing each of these steps, and for saving data along the way. See appendix C for an example processing script.

3.1 Reading data

ADV's typically record data internally in a compact vendor-defined binary format. The vendor will generally publish the details of the data format (e.g. Røstad, 2011), and also release software tools for viewing this data and/or writing it to other common data formats (e.g. white space-, comma- tab-delimited formats, MatlabTMformat, or other increasingly common standards such as HDF5).

Nortek provides software tools for converting raw/binary ‘.vec’ files to MatlabTM format (see <http://www.nortek-as.com/en/support/software>), and the DOLfYN software package is capable of reading these files directly into Python NumPy arrays (appendix C, line 40). A dataset will also generally need to be ‘cropped’ to the period of interest (e.g. when the instrument was in place on the seafloor, Figure 13).

3.2 Motion Correction

Raw turbulence measurements from moored ADV's will be contaminated by mooring motion. When IMU measurements are tightly synchronized with standard ADV velocity estimates, the IMU measurements can be used to reduce this contamination. This involves removing the measured velocity induced by ADV head-motion, \vec{u}_h^e , from the measured velocity, \vec{u}_m^e , to estimate the ‘motion corrected’ velocity in the earth frame,

$$\vec{u}^e(t) = \vec{u}_m^e(t) - \vec{u}_h^e(t) \quad . \quad (1)$$

Here superscript ‘e’ denotes the earth coordinate system.

We now break \vec{u}_h^e into two parts, $\vec{u}_h^e = \vec{u}_a^e + \vec{u}_\omega^e$. The first is an estimate of the linear motion of the ADV,

$$\vec{u}_a^e(t) = - \int \{ \vec{a}^e(t) \}_{HP(f_a)} dt \quad . \quad (2)$$

Here, $\vec{a}^e(t)$ is the IMU-measured acceleration signal rotated into the earth frame⁷, and $\{ \}_{HP(f_a)}$ denotes an appropriate high pass filter of frequency f_a . The acceleration must be high-pass filtered in this way to remove the influence of gravity and that of low-frequency bias (bias drift) that is inherent to IMU acceleration measurements (for further details see appendix B and Egeland (2014)).

⁷i.e. $\vec{a}^e(t) = \mathbf{R}^T(t) \cdot \vec{a}^*(t)$, see appendix A for details.

The second component of \vec{u}_h^c is due to rotational motion of the ADV-head about the IMU,

$$\vec{u}_\omega^c(t) = -\mathbf{R}^T(t) \cdot \left(\vec{\omega}^*(t) \times \vec{\ell}^* \right) \quad (3)$$

Here $\vec{\omega}^*$ is the IMU-measured rotation-rate, $\vec{\ell}^* = \vec{l}_{\text{head}}^* - \vec{l}_{\text{imu}}^*$ is the vector from the IMU to the ADV head, \times indicates a cross-product and superscript *s denotes a quantity in the ‘ADV body’ coordinate system. This coordinate system is used explicitly here to emphasize that $\vec{\ell}^*$ is constant in time. Matrix multiplication (denoted by ‘ \cdot ’) with the inverse ADV body orientation matrix, $\mathbf{R}^T(t)$, is used to rotate the ‘body-frame rotation induced velocity’ into the earth frame. For details on these coordinate systems and the definition of the orientation matrix see appendix A. The minus signs in equations (2) and (3) are correct because the measured velocity *induced by head motion* is in the opposite direction of the head motion itself.

All of the steps can be performed using DOLfYN’s `adv.io.rotate.CorrectMotion` class. To do this, you will need to specify \mathbf{H} and \vec{l}_{head}^* as ‘properties’ of your raw (cleaned) adv data object, and select a value for f_a (e.g. lines 18, 23, 34, 108-111 of appendix C). For those unfamiliar with Python, the ‘`motcorrect_vector.py`’ script bundled with DOLfYN provides a command-line interface for performing this motion correction and saves the motion-corrected data in Matlab™ format. In that case \mathbf{H} and \vec{l}_{head}^* are specified in an input ‘orient’ file, and f_a can be specified as a command-line option.

3.2.1 Select a local coordinate system

Prior to performing any averaging and computing other statistics it is often useful to rotate the measurements into a locally meaningful coordinate system. For the purposes of quantifying turbulence at HKT sites it is common practice to rotate the data into a coordinate system in which u is the ‘streamwise’ velocity, v is the ‘cross-stream’ velocity and w is in the ‘up’ direction. For details on selecting, estimating and transforming-into such a coordinate system see appendix A.2.

3.3 Cleaning data

Data ‘cleaning’ is a two-step process of 1) identifying erroneous (bad) points in an otherwise good dataset and 2) replacing them with either a) reasonable estimates of the values at those points, or b) ‘error values’ (e.g. NaN = ‘not-a-number’) which explicitly indicate the points are invalid. Several methods exist for identifying bad data. These include:

1. Search the data for manufacturer-defined ‘error values’ (if the manufacturer defines these⁸).
2. Search for values outside a reasonable range. For example, tidal velocities are typically less than 4m/s; therefore a velocity measurement greater than 5m/s is probably bad. Histograms can be useful for identifying the reasonable velocity range. The distribution of velocity measurements will often be approximately Gaussian; values well-beyond the tails of the distribution (>3 standard deviations) can probably be identified as bad.
3. Utilize diagnostic data from the instrument to identify bad data. For example, low values of ‘correlation’—the similarity of the send and receive acoustic pulses—can sometimes indicate bad data.
4. Apply ‘spike detection’ algorithms to the velocity signal. While turbulence is, by definition, unsteady and chaotic it is not discontinuous. Large and sharp spikes in the velocity signal are almost always bad.

Modern ADVs often produce data of sufficiently high quality that only a relatively small number of spike-type bad data points are present in the raw data (after cropping). In these cases spike-detection is usually sufficient to identify bad points. The recommended spike-identification method is documented in Goring and Nikora (2002) and Wahl (2003), and implemented in DOLfYN’s `adv.clean.GN2002` function.

⁸The velocity data in Nortek Vector (.vec) files do not contain an error value.

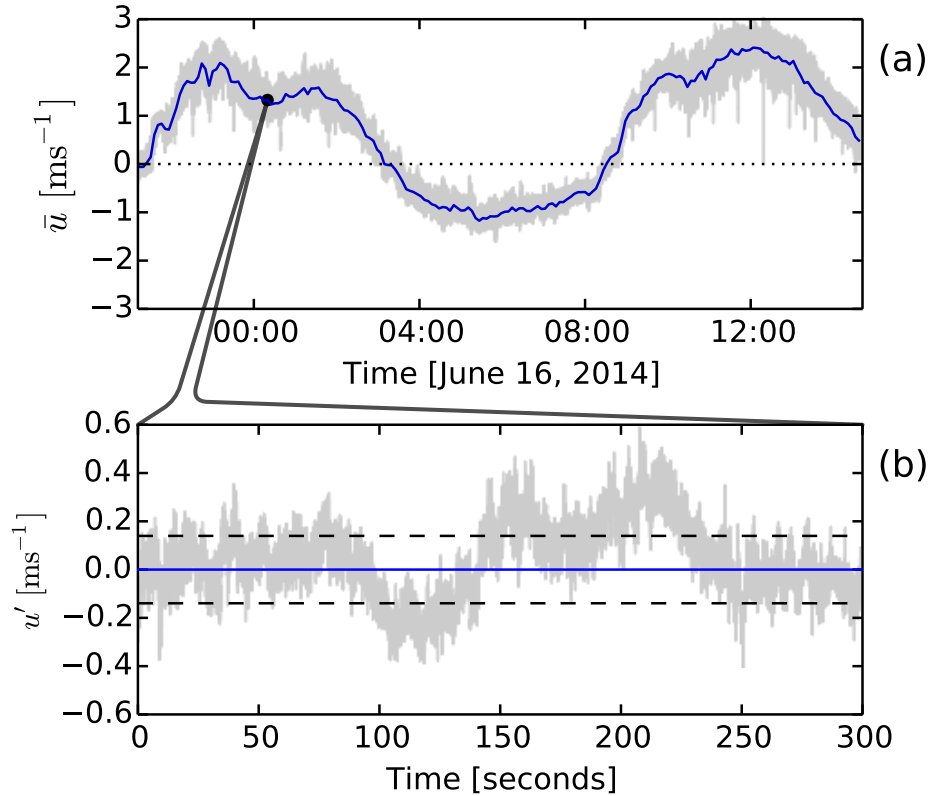


Figure 5. An example velocity time-series measured using a TTM at Admiralty Inlet. A) The mean stream-wise velocity (\bar{u} , blue, $\Delta t = 5\text{min}$) is over-layed on the full signal (grey). B) A 5min data window of the turbulent piece of the streamwise velocity, u' . The dashed lines indicate one standard deviation.

After points have been identified as bad they will need to be replaced. For cases of a small number of sparsely distributed bad data points they can be replaced with interpolated values (DOLfYN's `adv.clean.GN2002` function uses a least-squares cubic-polynomial) without introducing significant interpolation-related bias. This approach produces a dataset that can be further processed without the headache of dealing with NaN values.

If, on the other hand, there are segments of data with large fractions of bad points (>10-20%) interpolation may introduce significant bias to a myriad of statistics of the data. In these cases it is best to crop-out the bad segment (perhaps creating two distinct data sets that can be rejoined later), or to assign NaN values to the bad points. In general, the choice between these options will depend on the objectives of the analysis or the preference of the investigator. For the purposes of this document, in which spectral analysis is a primary result, assigning NaN values will make spectral analysis difficult to the point that it is best to simply split the data record to remove the bad segments and plan to recombine in later stages of processing.

3.4 Turbulence metrics and averaging

Having cleaned the raw data and computed an estimate of the velocity vector in a useful coordinate system, \vec{u} , one can finally begin estimating the turbulence statistics and average (mean) flow properties the measurements were designed to capture. For each component of velocity, $\vec{u} = (u, v, w)$, turbulence is defined by separating the instantaneous

velocity (e.g. u) into ‘average’ (\bar{u}) and ‘turbulent’ (u') pieces⁹,

$$u = \bar{u} + u' \quad (4)$$

Where the over-bar denotes a ‘suitable average’, over a period Δt , such that $\overline{u'} = 0$. For HKTs, it is useful to choose Δt such that \bar{u} is the flow which the turbine is designed to efficiently convert into useful energy, while the turbulence is what contributes to fatigue loads that decrease device lifetime. That is, Δt should be somewhat longer than a typical HKT ramp-up time (tens of seconds to a minute or two). Defined this way a turbine can be considered to be in a ‘steady operational state’ so long as changes in \bar{u} are small compared to \bar{u} itself. Turbulent velocity fluctuations can then be treated as disturbances to a HKT’s ‘steady operation’.

A time scale Δt must be chosen such that the tidal flow has stationary statistics (i.e., stable mean and variance) for that duration of tide. If Δt is too long, the tidal variation itself will contaminate the results. The wind energy industry uses $\Delta t = 10\text{min}$ (Commission, 2005). This is appropriate for large modern wind turbines (with long ramp-up times), but the smaller size of current HKTs suggests that they may respond faster and therefore that a smaller Δt might be appropriate (Gunawan et al., 2014). On the other hand, if turbulence is to be treated as the primary driver of device fatigue loads one should be careful not to implicitly neglect energetic low-frequency turbulence by selecting Δt to be too short.

With these considerations in mind, and until further work provides details on the relationship between turbulent inflow and HKT loads, this document recommends using $\Delta t = 2\text{-}10$ minutes. The exact choice of Δt —within this range—is unlikely to alter the results significantly, and should be adjusted depending on the goals of the analysis. For example, when fitting theoretical spectra to observations for the purpose of input to stochastic flow simulation tools such as TurbSim (Jonkman, 2009), it is desirable to include lower frequencies in the fit, and therefore it is reasonable to use a longer Δt (5-10min).

With Δt chosen the ADV data record is broken into segments in which turbulence statistics are computed. In this way the time-series of instantaneous velocity, \vec{u} (at the instrument sample rate, e.g. 16Hz), is converted to a time-series of turbulence statistics (with time-step Δt , Figure 5). It is recommended to save your data at this level to allow quick and easy access during analysis.

The remainder of this section defines several turbulence variables that are commonly used in the HKT industry and can be computed from moored ADV measurements. Furthermore, DOLfYN’s `adv.io.turbulence.TurbBinner` provides a two line interface for performing averaging and computing *all* of these statistics (e.g. lines 124-125 in appendix C).

3.4.1 Turbulence intensity

Turbulence intensity is used throughout the wind industry, and other engineering fields as a zeroth-order metric for quantifying turbulence. It is defined as the ratio of the standard deviation of horizontal velocity magnitude ($U = \sqrt{u^2 + v^2}$) to its mean,

$$I = \frac{\text{std}(U)}{\bar{U}}$$

Turbulence intensity is often quoted in units of percent (i.e. $100 \cdot I$). It is useful because it is easy to understand and—in many observations of atmospheric and oceanic turbulence—is relatively constant for $\bar{U} \gg 0$. On the other hand, I has often been criticized for being too simple (in particular that it only includes information about horizontal velocity) such that it does not provide enough information about the turbulence for various applications.

3.4.2 Turbulent kinetic energy

⁹Some discussions include a ‘wave velocity’ but, for simplicity, it is not included here at this time.

Turbulent kinetic energy (tke) quantifies the total energy contained in turbulence,

$$E_{tke} = \overline{u'u'} + \overline{v'v'} + \overline{w'w'}$$

Like I , E_{tke} , is useful because it is relatively simple. As a scalar quantity that includes all turbulence components, it has been studied at length by turbulence scientists and it has a well defined ‘budget’ equation that is the basis of turbulence theory. For some purposes it may be useful to investigate each component of E_{tke} individually. Lastly, it has sometimes been suggested that a turbulence intensity based on tke, that is $I_{tke} = \sqrt{E_{tke}}/\bar{U}$, would be more meaningful to engineering applications but this approach has not gained wide acceptance.

3.4.3 Reynold’s stresses

Reynold’s stresses are correlations between velocity components and are fundamentally important to turbulent flow fields. Unlike E_{tke} , Reynold’s stresses appear in the *mean*-flow equation explicitly as terms that transport (move) momentum from high velocity to low velocity regions. Because of how they appear in the mean-flow equation, Reynold’s stresses are typically treated as three distinct components, $\overline{u'v'}$, $\overline{u'w'}$, and $\overline{v'w'}$ ¹⁰. Several recent studies have found evidence that they are correlated with increased wind-turbine fatigue-loads (e.g. Kelley et al., 2002, 2005), which has begun to elevate their importance in the wind-energy field.

3.4.4 Turbulence auto-spectra

Turbulence velocity auto-spectra (hereafter, simply ‘spectra’) are estimates of the distribution of turbulent energy as a function of frequency. That is, a spectrum quantifies the amount of energy in the velocity at a range of time-scales. Furthermore, since time-scales can be converted into length scales using Taylor’s frozen flow hypothesis (i.e. $l_i = \bar{u}/f_i$), spectra quantify the distribution of turbulent energy at different length-scales. When considering turbulence to be a complex interaction of *eddies* from very small to very large scales, the spectrum quantifies the energy (rotation speed) of the eddies as a function of their size (δ , Figure 1).

HKTs respond to different scales of velocity fluctuations (different eddy sizes) differently. HKT simulation tools (such as Tidal Bladed, and HydroFAST¹¹) are capable of estimating the loads induced by these fluctuations, but the critical information of *how energetic* those fluctuations are, must be provided as input to these tools. Fortunately, spectra provide exactly this information: the distribution of energy as a function of eddy size.

Spectra are estimated from Fourier transforms (Fast Fourier Transforms) of the turbulent velocity,

$$S\{u\}(f) = |\mathcal{F}(u)|^2$$

In this work FFTs (denoted by $\mathcal{F}()$) are computed by removing a linear trend (fit) from u^{12} and applying hanning windows to reduce spectral reddening (Priestley, 1981). Spectra are normalized so that $\int S\{u\}(f)df = \overline{u'u'}$.

3.4.5 Spatial coherence

Spatial coherence is an estimate of the correlation of velocity components, over spatial distances, as a function of frequency. That is, where spectra indicate the energy in eddies as a function of their size (δ), coherence is an estimator of their ‘length’ (L). For 3D isotropic turbulence, these length scales should be similar. For the largest eddies, which are expected to be depth-limited and thus 2D anisotropic, it is likely that L will greatly exceed δ . Knowledge of the ‘length’ of these large eddies is important to HKT design because they are the most energetic and if their dimensions match that of HKT components they are likely to have a larger impact on the HKT.

¹⁰In many formalisms of turbulence the Reynold’s stresses are components of off-diagonal elements of the *Reynold’s stress tensor*. In these arenas the diagonal elements of that tensor are the components of E_{tke} .

¹¹Based on the NWTTC’s FAST wind-turbine simulation tool

¹²Note that removing a linear trend means that $\mathcal{F}(u) = \mathcal{F}(u')$.

The u -component spatial coherence is estimated as¹³,

$$\Gamma_{ij}\{u\}(f) = \frac{\langle |\mathcal{F}(u_i)\mathcal{F}(u_j)|^2 \rangle}{\langle S_i\{u\} \rangle \langle S_j\{u\} \rangle}$$

Where $\langle \rangle$ denotes an ensemble average, and i and j denote different measurement points in space.

4 Data analysis

Data analysis is the process of synthesizing useful knowledge or information from a set of data. The details of data analysis depend entirely on the goals of the analysis and the data available. That is, what question is attempting to be answered and how suitable is the dataset to answering that question? This section presents example analyses of moored-ADV data that provides potentially useful information for HKT site and device developers, and discussing the accuracy and limitations of the approach.

4.1 Initial inspection: time-series and histograms

As a first step in most analysis of velocity data, it is useful to plot the velocity and other turbulence statistics as a function of time. In the example data in Figure 6 the tidal currents reach 2m/s. During this period, at this location, the floods are significantly larger than the ebb. The mean velocity appears to be a reasonable estimate—there is a clear tidal signal, there are no sudden dramatic jumps in the values, and the magnitude of the velocity agrees with previous measurements at this site—this gives us confidence that our methods have produced a reliable dataset (Figure 6A).

The instantaneous turbulence intensity has an average of 10%, but approaches 20% in some 5-min periods (6B). As is often observed in turbulent flows throughout the oceans and atmosphere the turbulence is highly intermittent, that is it is dominated by large spikes and periods of relative calm (6C). Note also that the turbulence is significantly lower for the small ebb than it is for the two (larger) floods. The Reynold’s stresses show a similar pattern (6D).

HKT site-developers often use histograms of velocity measurements to estimate the available power at a tidal energy site. The record in Figure 6 isn’t long enough to estimate *annual energy production*, or AEP, but a histogram of the measurements does provide some indication of the distribution of velocity at the site (Figure 7). During this time period, for example, more than 30% of the measurements had a \bar{U} in the range of 0.8-1.2m/s.

4.2 Turbulence Spectra

The primary purpose for making ADV measurements at HKT sites is to measure the turbulence spectra. That is, ADVs resolve the inflow at a level of detail that cannot be measured with profiling instruments. Turbulence spectra are estimates of the distribution of energy as a function of frequency (eddy size). Because spectra reveal detailed information about the signal (velocity) they also reveal detailed sources of error in the measurement. It is therefore important to be aware of these errors so that one can be careful to exclude them from estimates of statistics meaningful to the flow.

Kolmogorov’s theory of locally isotropic turbulence predicted that turbulence spectra would have an ‘inertial sub-range’ in which the amplitude of the spectral components (i.e. $S\{u\}$, $S\{v\}$ and $S\{w\}$) will be equal, and in which the spectra will decay as $k^{-5/3}$ (Kolmogorov, 1941). This prediction has been confirmed by observation so ubiquitously in oceanic and atmospheric turbulence that it has become a defining characteristic of turbulence spectra (e.g. Figure 8A, data from Thomson et al. (2012)). Based on this we expect that deviations from this behavior are likely to indicate some source of error.

¹³Equivalent expressions apply for the v and w components.

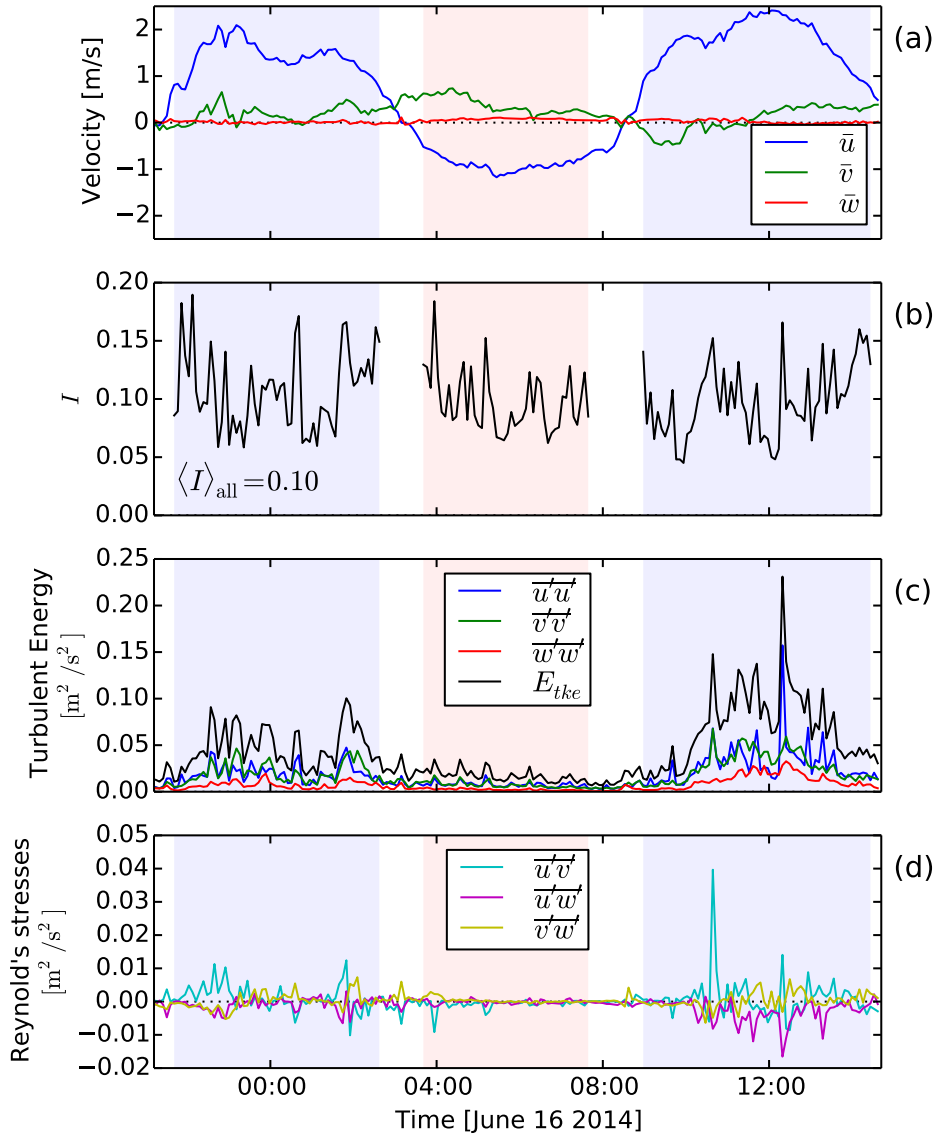


Figure 6. A time-series of turbulence statistics measured from a TTM at Admiralty Head: a) velocity, b) turbulence intensity, c) turbulent kinetic energy and its components, d) Reynold's stresses. Shaded regions indicate ebb (red) and flood (blue) periods where $U > 0.7$. Turbulence intensity is only plotted during these periods because it is meaningless for small values of U . The mean I over the data record is 10%.

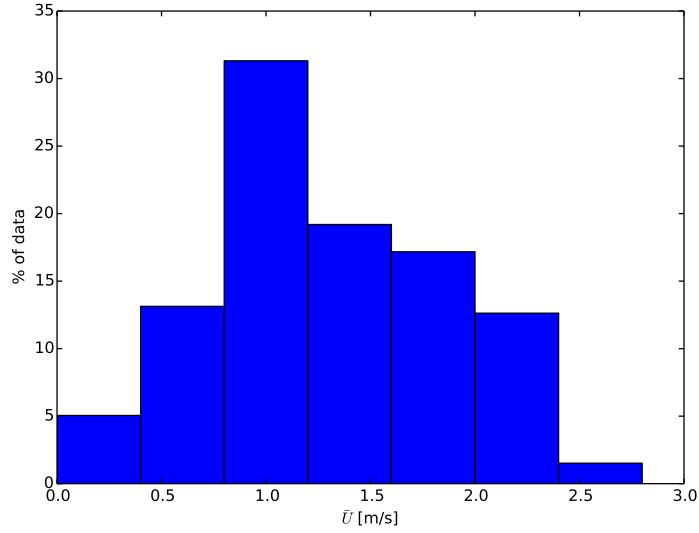


Figure 7. A histogram of the mean horizontal velocity magnitude.

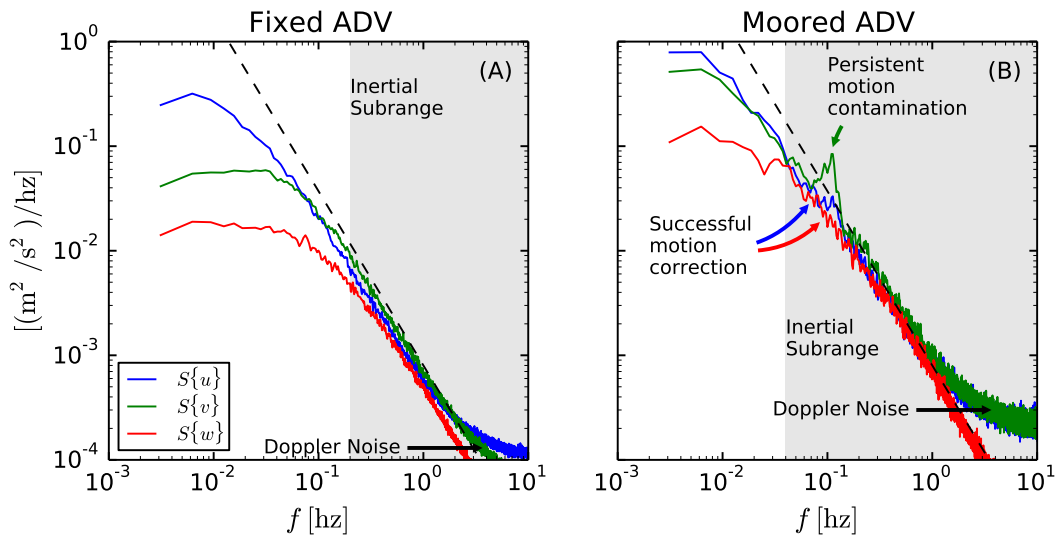


Figure 8. A comparison of the shape of spectra at two different sites from ADVs on a rigid tripod (A) and a TTM (B). The spectra for each velocity component, u , v , w are in blue, green and red, respectively. The shaded region indicates the ‘inertial subrange’, in which the spectra decay like $f^{-5/3}$ and all components have nearly the same amplitude. The dashed line indicates a $f^{-5/3}$ slope. The difference in amplitude of the spectra (between A and B) is expected because the turbulence measurements were made at different sites. In each panel the ‘doppler noise’ level arrow points at doppler noise that exceeds the high-frequency turbulence levels.

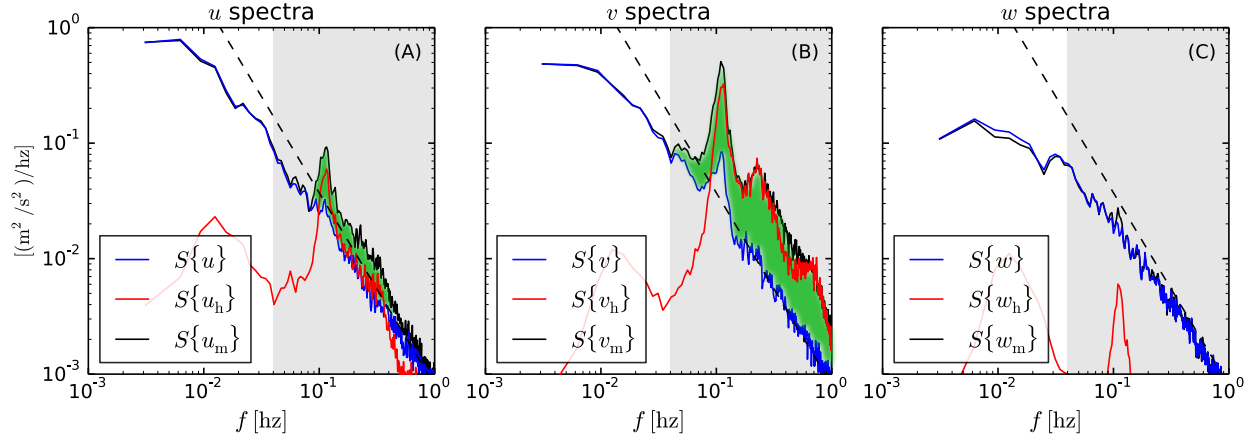


Figure 9. Spectra of turbulence highlighting motion correction. A) Streamwise velocity, B) cross-stream velocity, C) vertical velocity. Black lines show the uncorrected spectra, red show spectra of head motion, and blue shows the spectra after motion correction. Green shading highlights locations where motion correction reduced the spectral amplitude. The u and v spectra have sharp peaks at 0.1Hz—and lesser peaks at higher frequencies—that match the spectrum of \bar{u}_h^c , indicating motion-contamination. Motion correction removed the vast majority of the contamination from these spectra, but contamination from the large peak in the v spectra at 0.1Hz persists. The w spectra is essentially uncontaminated by the mooring motion. The inertial sub-range is shaded as it was in Figure 8.

There are two primary sources of error in moored ADV spectra: 1) Doppler noise, and 2) imperfect motion correction. Doppler noise has been studied at length and is easy to identify and account for. Doppler noise is a low-energy ‘white-noise’¹⁴ that results from uncertainty in the doppler-shift recorded by the ADV. In measurements of oceanic turbulence it is generally observed at high frequencies, where the amplitude of the turbulent motions drops below the ‘doppler noise level’ (Figure 8).

Estimates of $S\{v\}$ from a TTM show a peak near 0.1Hz that deviates from the $f^{-5/3}$ spectral slope (Figure 8B). Closer comparison of the velocity spectra to the spectra of uncorrected velocity measurements, $S\{\bar{u}_m^c\}$, and spectra of the head-motion, $S\{\bar{u}_h^c\}$, shows that this peak is indeed due to mooring motion (Figure 9). This comparison is remarkable because it highlights the effectiveness of the motion correction method. At many frequencies, head motion is $5\times$ larger than the corrected signal (which is believed to be correct because it agrees with a $f^{-5/3}$ spectral slope). Furthermore—with the understanding of isotropy and the $f^{-5/3}$ slope—there is a strong theoretical footing to simply interpolate over the peak in $S\{v\}$ to estimate the underlying real spectrum. These results suggest that motion-corrected moored ADV measurements are capable of producing accurate estimates of all three components of the turbulence spectra.

4.3 Spatial Coherence

Spatial coherence is the highest-order turbulence statistic that is considered in this document. As such, it is highly sensitive to the details of the inflow and measurement method. Methods for measuring this variable over the scales important to HKTs (e.g. rotor diameter) permit inflow simulations that accurately resolve the spatial correlations of turbulence at HKT sites.

Vertical spatial coherence estimates from two IMU-equipped ADVs deployed on a TTM, separated by 0.6m, are plotted in Figure 10A. The lack of motion contamination in $S\{w_m\}$ (Figure 9), suggests that this component will have an accurate estimate of $\Gamma_{\Delta z}\{w\}$. Indeed, the shape of $\Gamma_{\Delta z}\{w\}$ agrees with measurements of coherence from

¹⁴White noise has constant amplitude with frequency.

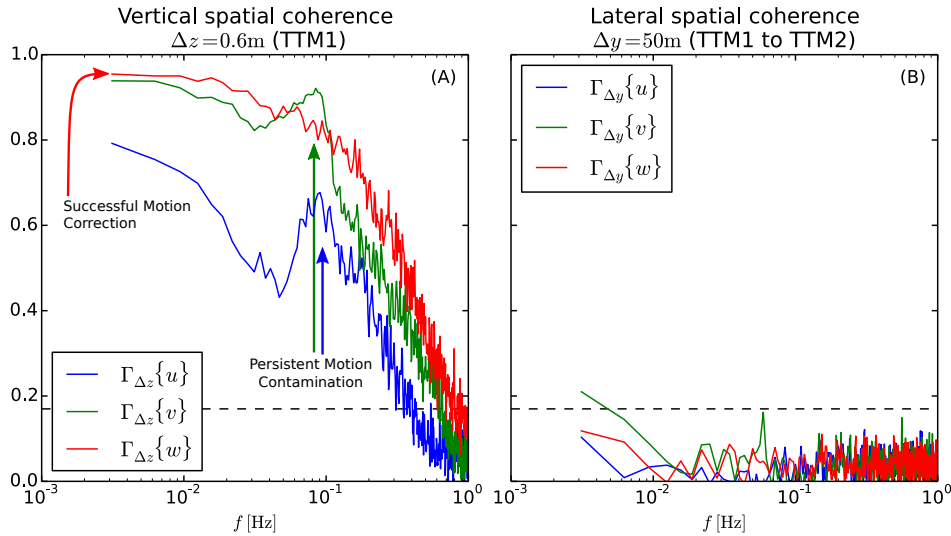


Figure 10. Spatial coherence estimates from TTMs. Vertical coherence estimates (A) are from ADVs on TTM1 spaced 0.6m apart. Lateral coherence estimates (B) are between neighboring TTMs spaced 50m apart. Dashed lines in both figures indicate the 95% confidence level above which the coherence estimates are statistically different from 0.

other environments (i.e. it has an exponential decay, Kilcher et al. (2014)). Unfortunately $\Gamma_{\Delta z}\{u\}$ and $\Gamma_{\Delta z}\{v\}$ are contaminated by persistent mooring-motion contamination at 0.1Hz. The peak in coherence arises because the measurements were made from the same TTM strongback-vane and the co-motion of that vane created a peak in the coherence estimate at the frequency of mooring motion.

The lateral spatial-coherence estimates between ADVs on two different TTMs shows zero-spatial coherence. We believe this to be a reliable and important result: at this site (50m water depth) and distance above the bottom (11m) turbulence is incoherent over spatial separations of 50m. This supports the theory that the limiting scale for spatial coherence of turbulence is controlled by the outer scale of the forcing. That is, the lateral spatial coherence is controlled by the distance from the bottom. This indicates that turbulent loading on devices in an array with hub-heights smaller than their separation distance will be uncorrelated across the array.

5 Summary

This document outlines the methods for making turbulence measurements at HKT sites using mooring-deployed IMU-equipped ADVs. The critical issue addressed by this approach is that ADVs—which accurately measure turbulence statistics—are deployed at heights above the sea-bed that are relevant to HKTs. Other existing approaches—most of which deploy instrumentation on the seafloor (either ADPs, or ADVs)—do not resolve the statistics of the turbulence with sufficient accuracy (ADPs) or at the correct location (ADVs) to produce reliable device lifetime estimates.

This manual provides guidance on: 1) designing mooring hardware that can support the instrumentation, 2) planning deployment and recovery to capture the statistics of turbulence that are important to HKTs, 3) configuring instrumentation for data collection, 4) processing data, and 5) tips for analyzing data to produce useful results. It is highly recommended that users of this manual also download and install the DOLFIN software package, as each data processing step described herein can be performed in a few lines of code. In particular, the tedious details of accounting for different coordinate systems have been simplified therein (appendix A).

Finally, in section 4, we demonstrate analysis methods for producing estimates of turbulent quantities that are use-

ful to HKT device and site developers. Most importantly, the approach outlined in this method produces reliable estimates of the Reynold's stresses, turbulent energy, and turbulence spectra. The w -component of vertical spatial coherence can be estimated from a single mooring, and the research team behind this manual is developing a new, more stable platform for measuring the u - and v -components of spatial coherence.

Feedback

If you have comments, questions, suggestions or corrections please contact Levi Kilcher at the National Renewable Energy Laboratory. He will be happy to address your concerns if time and resources permit. Send comments to:

Levi Kilcher
NWTC/3811
National Renewable Energy Laboratory
1617 Cole Blvd
Golden, CO 80401-3393
United States of America
levi.kilcher@nrel.gov
+1 (303) 384-7192

References

- Commission, I.E. (2005). Wind Turbines Part 1: Design requirements.
- Egeland, M.N. (2014). *Spectral evaluation of motion compensated adv systems for ocean turbulence measurements*. Ph.D. Thesis, Florida Atlantic University.
- Goring, D.G.; Nikora, V.I. (2002). “Despiking acoustic doppler velocimeter data.” *Journal of Hydraulic Engineering* 128; pp. 117–126.
- Gunawan, B.; Neary, V.S.; Colby, J. (2014). “Tidal energy site resource assessment in the East River tidal strait, near Roosevelt Island, New York, NY (USA).” *Renewable Energy* 71; pp. 509–517.
- Jonkman, B.J. (September 2009). *TurbSim user’s guide version 1.50*. NREL/TP-500-46198, National Renewable Energy Laboratory.
- Kelley, N.; Hand, M.; Larwood, S.; McKenna, E. (January 2002). *The NREL Large-Scale Turbine Inflow and Response Experiment - Preliminary Results*. NREL/CP-500-30917, National Renewable Energy Laboratory.
- Kelley, N.D.; Jonkman, B.J.; Scott, G.N.; Bialasiewicz, J.T.; Redmond, L.S. (August 2005). *The impact of coherent turbulence on wind turbine aeroelastic response and its simulation*. NREL/CP-500-38074, National Renewable Energy Laboratory.
- Kilcher, L.; Thomson, J.; Colby, J. (April 2014). “Determining the spatial coherence of turbulence at MHK sites.” *2nd Marine Energy Technology Symposium*. Seattle, WA.
- Kolmogorov, A.N. (1941). “Dissipation of Energy in the Locally Isotropic Turbulence.” *Dokl. Akad. Nauk SSSR* 32(1); pp. 16–18.
URL <http://links.jstor.org/sici?sici=0962-8444%2819910708%29434%3A1890%3C15%3ADOEITL%3E2.0.CO%3B2-C>
- MicroStrain, I. (). *3DM-GX3-25 Miniature Attitude Heading Reference system product datasheet*. LORD Microstrain.
URL <http://files.microstrain.com/3DM-GX3-25-Attitude-Heading-Reference-System-Data-Sheet.pdf>
- (April 2012). *3DM-GX3-15,-25 MIP Data Communications Protocol*. 459 Hurricane Lane, Williston, VT 05495. www.microstrain.com/inertial/3DM-GX3-25/.
URL <http://files.microstrain.com/3DM-GX3-15-25-MIP-Data-Communications-Protocol.pdf>
- Nortek (August 2005). *Vector Current Meter User Manual*. Vangkroken 2, NO-1351 RUD, Norway, h ed.
- Polagye, B.; Thomson, J. (2013). “Tidal energy resource characterization: methodology and field study in Admiralty Inlet, Puget Sound, WA (USA).” *Proceedings of the Institution of Mechanical Engineers, Part A: Journal of Power and Energy* 227(3); pp. 352–367.
- Priestley, M. (1981). *Spectral Analysis and time series*. Academic Press.
- Røstad, J. (September 2011). *System Integrator Manual*. Nortek AS, Vangkroken 2, NO-1351 RUD, Norway.
- Stacey, M.T.; Monismith, S.G.; Burau, J.R. (1999). “Observations of Turbulence in a Partially Stratified Estuary.” *Journal of Physical Oceanography* 29; pp. 1950–1970.
- Thomson, J.; Kilcher, L.; Richmond, M.; Talbert, J.; deKlerk, A.; Polagye, B.; Guerra, M.; Cienfuegos, R. (2013). “Tidal turbulence spectra from a compliant mooring.” *1st Marine Energy Technology Symposium*. Washington, DC.

Thomson, J.; Polagye, B.; Durgesh, V.; Richmond, M. (2012). "Measurements of turbulence at two tidal energy sites in Puget Sound, WA." *Journal of Oceanic Engineering* 37(3); pp. 363–374.

Wahl, T.L. (2003). "Discussion of "Despiking Acoustic Doppler Velocimeter Data" by Derek G. Goring and Vladimir I. Nokora." *Journal of Hydraulic Engineering* 129; pp. 484–487.

A Coordinate systems

Tracking coordinate systems (‘reference frames’, or simply ‘frames’) is a critical and somewhat tedious task for making accurate velocity measurements using moored ADVs. The coordinate systems for doing so can be broken into two categories: 1) the ‘inertial’ or ‘stationary’ ones into which it is the goal to transform the measurements, and 2) the moving coordinate systems in which sensors make measurements. The purpose of this appendix is to clearly document and define the relationships between all of the coordinate systems necessary for quantifying turbulence using moored ADVs. This appendix starts with general definitions of coordinate systems and the relationships between them (A.1), then details the stationary and measurement frames used herein (A.2 and A.3, respectively).

A.1 Defining coordinate systems

Consider two three-dimensional right-handed coordinate systems (‘a’ and ‘b’) with orthogonal basis vectors \hat{x}^a , \hat{y}^a , \hat{z}^a , and \hat{x}^b , \hat{y}^b , \hat{z}^b . In general, these coordinate systems are related by the equation:

$$\vec{r}^b = \mathbf{R}_b^a \cdot (\vec{r}^a - l_b^a)$$

Here superscripts denote the coordinate system that the quantity is measured in and \cdot indicates standard matrix multiplication. The vectors \vec{r}^a and \vec{r}^b point to the same point in space, but in the two distinct coordinate systems. In this framework the vector l_b^a is the ‘translation vector’ that specifies the origin of coordinate system ‘b’ in the ‘a’ frame, and \mathbf{R}_b^a is the ‘orientation matrix’ of ‘b’ in ‘a’. With these definitions, the following statements are true:

- a vector can be mapped from one coordinate system to the other by,

$$\vec{u}^b = \mathbf{R}_b^a \cdot \vec{u}^a$$

- The inverse rotation is simply the transpose,

$$\mathbf{R}_a^b = (\mathbf{R}_b^a)^{-1} = (\mathbf{R}_b^a)^T$$

- The determinant of the rotation matrix is 1,

$$\det(\mathbf{R}_b^a) = 1$$

A.2 Stationary frames

Throughout the main body of this document measurements are discussed in terms of two stationary coordinate systems: a) the ‘earth frame’ is the coordinate system in which motion correction is performed¹⁵, and b) a local ‘analysis frame’ coordinate system in which turbulence is analyzed and discussed.

A.2.1 The earth frame

The earth coordinate system is the coordinate system in-which the orientation of the ADV is measured (see A.3.2), and is the coordinate system in-which motion correction is most easily calculated and discussed (section 3.2). This work utilizes ‘e’ superscripts to denote an ‘ENU’ earth coordinate system with basis vectors,

\hat{x}^e : East,

\hat{y}^e : North, and

\hat{z}^e : Up.

¹⁵No doubt the earth reference frame is not technically ‘inertial’, but for the purposes of measuring turbulence in tidal straits we consider it to be so.

A.2.2 The analysis frame

The choice of ‘analysis frame’ will, in general, depend on the data available and the goals of the analysis. For quantifying inflow to HKTs it is common practice to use a coordinate system in which,

\hat{x} : is the ‘streamwise’ or ‘flood’ direction,

\hat{y} : is the ‘cross-stream’ direction (defined by the right-hand rule relative to \hat{x} and \hat{z}), and

\hat{z} : is the ‘vertical up’ direction.

Note that throughout this work vector quantities with *no superscript* are in this local frame. The orientation of this frame relative to the earth is defined as,

$$\mathbf{S}^e = \begin{pmatrix} \cos \theta & \sin \theta & 0 \\ -\sin \theta & \cos \theta & 0 \\ 0 & 0 & 1 \end{pmatrix}$$

Where θ is the angle from East to the ‘streamwise’ direction.

For the purpose of estimating θ it is convenient to use complex notation for the horizontal velocity,

$$\tilde{U}^e = u^e + iv^e = U e^{i\phi^e}$$

Where $i = \sqrt{-1}$, $e \approx 2.71828$ is Euler’s number, U is the instantaneous horizontal velocity magnitude and ϕ^e is the angle of that velocity from east.

For measurements at locations where the flow does not change direction dramatically over the measurement period (e.g. in rivers), the streamwise direction can be estimated simply from an average of the horizontal velocity over the entire data record,

$$\theta_{\text{river}} = \arg(\langle \tilde{U}^e \rangle_{\text{data}})$$

Where $\langle \rangle_{\text{data}}$ denotes an average of all data, and \arg returns the complex angle of its argument.

For measurements at locations where velocity changes direction over the measurement period a more sophisticated method for determining a local coordinate system is often required. For tidal flows, for example, it is often useful to define the ‘streamwise’ direction to be parallel with ebb and opposite flood (or vice-versa). This can be done by first defining,

$$\phi^\dagger = \begin{cases} 2\phi^e & \text{for } 0 < \phi^e < \pi \\ 2(\phi^e - \pi) & \text{for } \pi < \phi^e < 2\pi \end{cases}$$

That is, ϕ^e angles in the lower-half of the unit circle are rotated to be in the opposite direction, and then all angles are doubled so that ϕ^\dagger ‘fills-out’ the unit circle again. When re-combined with the velocity magnitudes, ϕ^\dagger , can be used to estimate the ebb-flood direction as,

$$\theta_{\text{tide}} = \arg(\langle U e^{i\phi^\dagger} \rangle_{\text{data}}) / 2$$

The ambiguity over whether θ_{tide} points in the direction of ebb or flood can easily be resolved by knowledge of the tidal-geographic context of the measurements.

A.3 Measurement frames

To combine signals from an IMU with those of an ADV to perform motion correction the coordinate systems in which each of the measurements are made must be carefully accounted for.

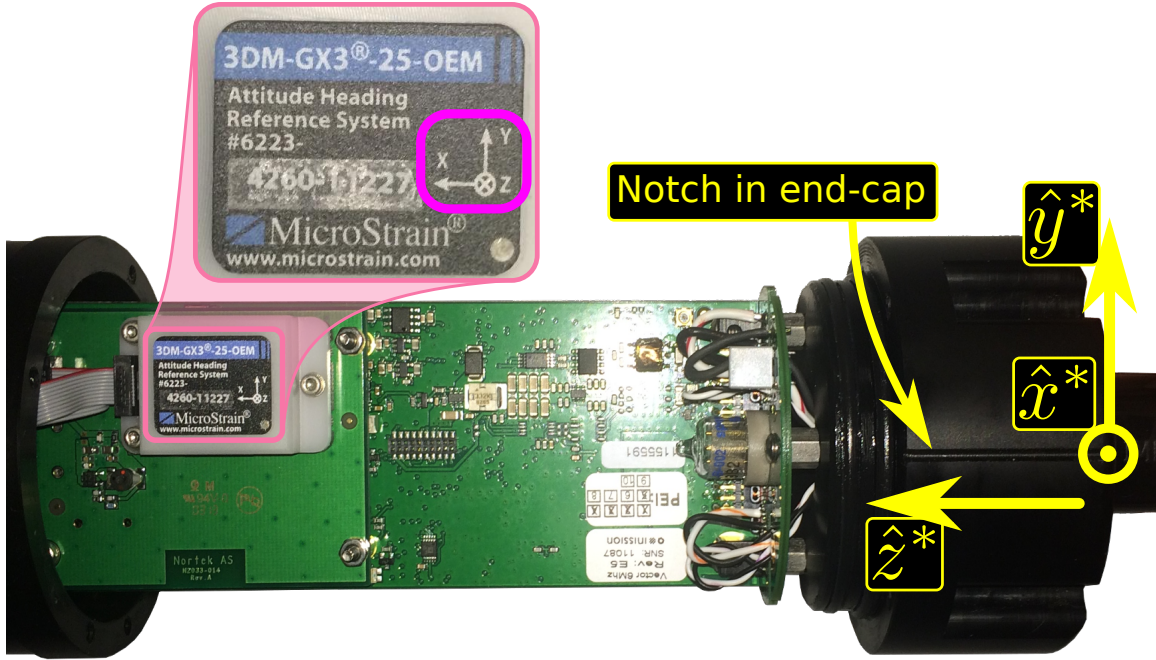


Figure 11. The circuit-board and pressure-case end-cap of a Nortek Vector equipped with a Microstrain IMU. The ADV-body coordinate system (yellow) is depicted on the right. The notch in the end-cap defines the \hat{x}^* direction (out of the page), and the \hat{z}^* direction points back along the pressure case axis. A zoom-in on the Microstrain chip highlights its coordinate system (magenta) relative to the body.

For the Nortek Vector instruments that were used for this work the ‘ADV-body’ coordinate system is defined as being centered on the cylinder-body axis at the point where the head-cable meets its end-cap. The basis vectors of this coordinate system are defined as (Figures 11 and 12B):

\hat{x}^* : points from the center of the ‘head’ end-cap toward the notch in that end-cap,

\hat{y}^* : is defined by the right-hand-rule based on the other two basis vectors, and

\hat{z}^* : points from the ‘head’ end-cap toward the ‘battery’ end-cap along the body-cylinder (pressure case) axis.

A.3.1 The ADV head

In order to transform measured velocities into a meaningful reference frame (and to perform motion correction) the orientation (and position) of the ADV head in terms of the body coordinate system must be known. To facilitate this the orientation matrix of the ADV head, \mathbf{H} , and translation vector¹⁶, \vec{l}_{head}^* , are defined according to,

$$\vec{x}^{\text{head}} = \mathbf{H} \cdot (\vec{x}^* - \vec{l}_{\text{head}}^*) \quad , \quad (5)$$

where \vec{x}^{head} and \vec{x}^* are the same point in the head and body coordinate systems, respectively. Combined with the math notes in the previous section, the velocity vectors in the head frame can be transformed into the body frame by,

$$\vec{u}^* = \mathbf{H}^T \cdot \vec{u}^{\text{head}} \quad . \quad (6)$$

For Nortek Vectors, the coordinate system of the ADV head is centered on the transmit transducer face, and the coordinate-directions are defined by (Figure 12B, Nortek (2005)):

¹⁶The position of the ADV-head origin (transmit transducer) in the body coordinate system.

\hat{x}^{head} : the direction of one of the transducer ‘receive’ arms (marked with tape or paint)

\hat{y}^{head} : is defined by the right-hand-rule based on the other two basis vectors, and

\hat{z}^{head} : is into the transducer face.

For fixed-head Nortek Vector ADVs, the body-frame and head-frame have parallel coordinate systems (\mathbf{H} is the identity matrix), and the ‘head-frame’ is translated 21cm along the z -axis. That is, $\vec{l}_{\text{head}}^* = (0, 0, -0.21)\text{m}$ (Nortek, 2005).

For cable-head ADVs, the position and orientation of the ADV head is arbitrary. This means that when preparing to make measurements using cable-head ADVs, **the orientation and position of the ADV head must be accurately recorded** in order to allow the ADV measurements to be transformed into the body frame during post-processing. For the example in Figure 12A, $\vec{l}_{\text{head}}^* = (254, 64, -165)\text{mm}$, and

$$\mathbf{H} = \begin{pmatrix} 0 & 0 & -1 \\ 0 & -1 & 0 \\ -1 & 0 & 0 \end{pmatrix} .$$

In general \mathbf{H} will not necessarily be symmetric nor will it have so many zero-elements (i.e. these characteristics are specific to the head-body alignment of the example).

A.3.2 The IMU coordinate system

Like the ADV head, the coordinate system in which the IMU measurements are made must be clearly defined and documented. In general, the IMU frame is related to the body coordinate system by,

$$\vec{x}^{\text{imu}} = \mathbf{A} \cdot (\vec{x}^* - \vec{l}_{\text{imu}}^*) .$$

For the Microstrain 3DM-GX3-25 (IMU) as it is integrated into the Nortek Vector (Figure 11), $\vec{l}_{\text{imu}}^* = (0.006, 0.006, 0.150)\text{m}$ and,

$$\mathbf{A} = \begin{pmatrix} 0 & 0 & 1 \\ 0 & 1 & 0 \\ -1 & 0 & 0 \end{pmatrix} .$$

The DOLfYN software package automatically rotates all IMU vectors so that orientation and motion data returned by `dolfyn.io.read_nortek` is in the ADV body frame (see the `dolfyn.io.nortek.NortekReader.sci_microstrain` source code for details). DOLfYN also adds \vec{l}_{imu}^* to \vec{l}_{head}^* to estimate \vec{l}^* .

The orientation matrix

In order to use the orientation matrix to rotate velocity measurements into an earth-fixed coordinate system it is important to understand how the orientation matrix is defined. The Microstrain IMU outputs an orientation matrix, \mathbf{R}_{imu} , such that:

$$\vec{u}^{\text{imu}} = \mathbf{R}_{\text{imu}} \cdot \vec{u}^{\text{NED}} .$$

Where \vec{u}^{imu} and \vec{u}^{NED} are vectors in the IMU’s local coordinate system and a ‘north-east-down’ (NED) earth-fixed coordinate system, respectively (MicroStrain, 2012). However, this NED earth coordinate system is different from the ENU earth coordinate system used here (and typically used by Nortek (Røstad, 2011)). That is,

$$\vec{u} = \mathbf{B} \cdot \vec{u}^{\text{NED}} ,$$

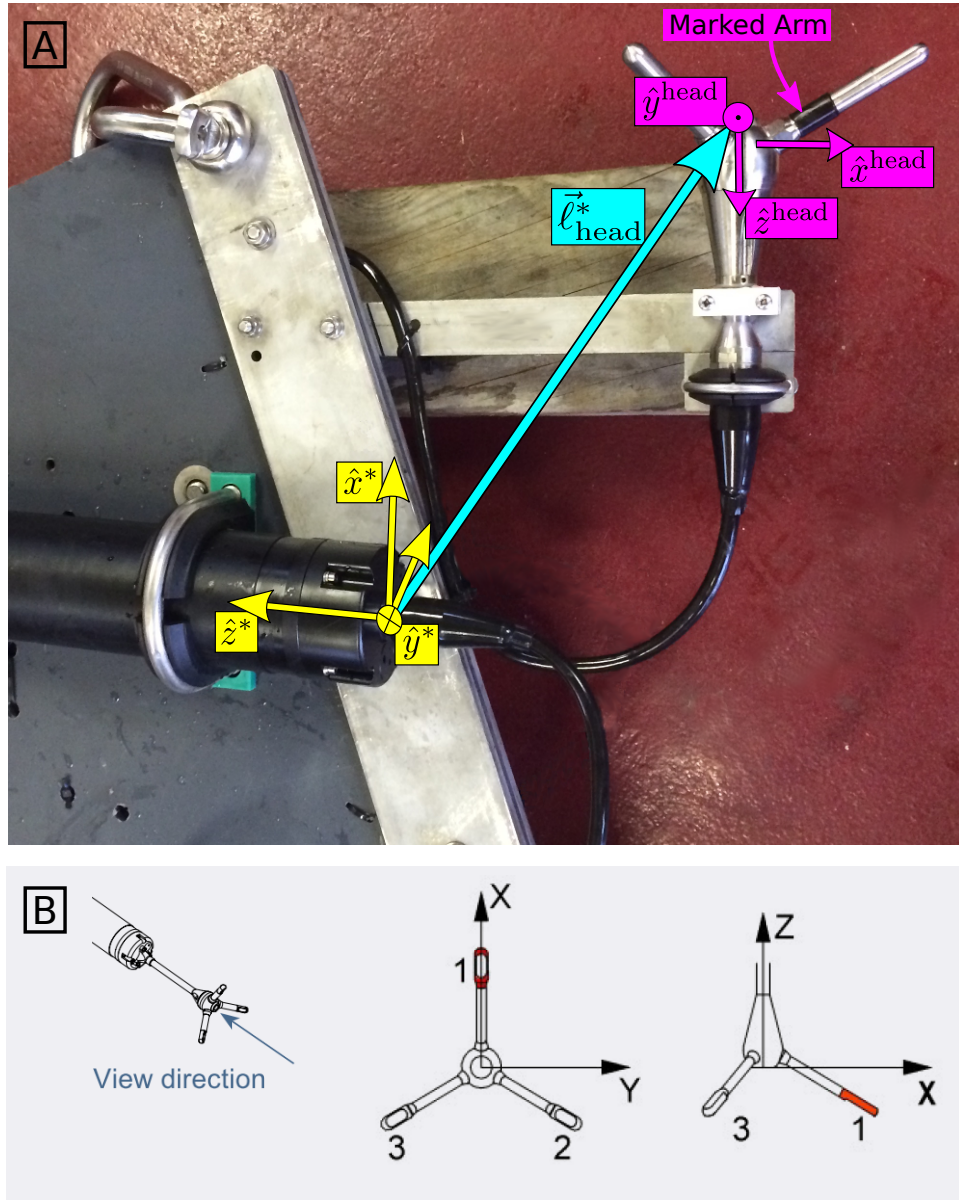


Figure 12. Coordinate systems of the ADV body and head. A) A strongback with an ADV rests on a block of wood. Coordinate systems of the ADV head (magenta) and body (yellow) are shown. The \hat{x}^{head} -direction is known by the black-band around the transducer arm, and the \hat{x}^* direction is marked by a notch on the end-cap (indiscernible in the image). The cyan arrow indicates the body-to-head vector, $\vec{\ell}_{\text{head}}^*$. The perspective slightly distorts the fact that $\hat{x}^{\text{head}} \parallel -\hat{z}^*$, $\hat{y}^{\text{head}} \parallel -\hat{y}^*$, and $\hat{z}^{\text{head}} \parallel -\hat{x}^*$. B) Coordinate system of the ADV head as defined in the Nortek Vector manual (Nortek, 2005).

where,

$$\mathbf{B} = \begin{pmatrix} 0 & 1 & 0 \\ 1 & 0 & 0 \\ 0 & 0 & -1 \end{pmatrix} .$$

From this, and the above discussion of the orientation of the IMU in the ADV, it is simple to show that the orientation matrix of the ADV body in a ENU earth frame is,

$$\mathbf{R} = \mathbf{A} \cdot \mathbf{R}_{\text{imu}} \cdot \mathbf{B} ,$$

The DOLfYN software package makes this transformation when reading the orientation matrix from Nortek Vector *.vec* files (i.e. the *'orientmat'* attribute in the data object returned by DOLfYN's *io.read_nortek* is \mathbf{R} , not \mathbf{R}_{imu}). This way vectors in the body frame can be rotated into the ENU earth frame by,

$$\vec{u} = \mathbf{R}^T \cdot \vec{u}^* .$$

B Filtering Acceleration

Bench-tests of the Microstrain IMU indicate that its accelerometers drift for frequencies $< 10^{-2}\text{Hz}$ (a minute or more, Egeland (2014)). Therefore, in order to remove bias-drifts in \vec{a} that—when integrated according to (2)—lead to large errors in \vec{u}_a^e this document recommends using $f_a = 0.033\text{Hz}$ (30seconds). On the other hand, real motions at and below f_a will not be accurately accounted for in \vec{u}_a^e , and will therefore persist as low-frequency motion contamination not corrected-for in the estimate of \vec{u} .

For moorings whose low-frequency motion is limited by the mooring line itself this is a reasonable approach. Assuming that the displacement of the ADV head (from the mooring’s neutral position) is likely to be $< 20\%$ of its distance from the bottom, then for ADVs deployed at 10m depth the speed of their low-frequency motion (i.e. below $f_a = 0.03\text{ Hz}$) will be $< 0.07\text{m/s}$. In other words, for a 10m mooring the choice of $f_a = 0.03\text{Hz}$ allows for low-frequency motion contamination on the order of 7cm/s to persist. This is a notable but relatively minor level of uncertainty in the context of the highly energetic flows that exist at tidal energy sites.

C DOLfYN data processing scripts

The following script details data processing steps.

adv_example01.py

```
1 # To get started first import the DOLfYN 'adv' advanced programming
2 # interface (API):
3 from dolfyn.adv import api as adv
4
5 # Import matplotlib tools for plotting the data:
6 from matplotlib import pyplot as plt
7 from matplotlib import dates as dt
8 import numpy as np
9
10 #####
11 # User input and customization
12
13 # The file to load:
14 fname = './data/vector_data_imu01.vec'
15
16 # This is the vector from the ADV head to the body-frame, in meters,
17 # in the ADV coordinate system.
18 body2head_vec = np.array([0.48, -0.07, -0.27])
19
20 # This is the orientation matrix of the ADV head relative to the body.
21 # In this case the head was aligned with the body, so it is the
22 # identity matrix:
23 body2head_rotmat = np.eye(3)
24
25 # The time range of interest.
26 t_range = [
27     # The instrument was in place starting at 12:08:30 on June 12,
28     # 2012.
29     dt.date2num(dt.datetime.datetime(2012, 6, 12, 12, 8, 30)),
30     # The data is good to the end of the file.
31     np.inf]
32
33 # This is the filter to use for motion correction:
34 accel_filter = 0.1
35
36 # End user input section.
37 #####
38
39 # Read a file containing adv data:
40 dat_raw = adv.read_nortek(fname)
41
42 # Crop the data for t_range using DOLfYN's 'subset' method (creates a
43 # copy):
44 t_range_inds = (t_range[0] < dat_raw.mpltime) & (dat_raw.mpltime < t_range[1])
45 dat = dat_raw.subset(t_range_inds)
46
47 # Then clean the file using the Goring+Nikora method:
```

```

48 adv.clean.GN2002(dat)
49 dat_cln = dat.copy()
50
51 #####
52 # Create a figure for comparing screened data to the original.
53 fig = plt.figure(1, figsize=[8, 4])
54 fig.clf()
55 ax = fig.add_axes([.14, .14, .8, .74])
56
57 # Plot the raw (unscreened) data:
58 ax.plot(dat_raw.mpltime, dat_raw.u, 'r-')
59
60 # Plot the screened data:
61 ax.plot(dat.mpltime, dat.u, 'g-')
62 bads = np.abs(dat.u - dat_raw.u[t_range_inds])
63 ax.text(0.55, 0.95,
64         "%0.2f%% of the data were 'cleaned' \nby the Goring+Nikora method." %
65         (np.float(sum(bads > 0)) / len(bads) * 100),
66         transform=ax.transAxes,
67         va='top',
68         ha='left',
69         )
70
71 # Add some annotations:
72 ax.axvspan(dt.date2num(dt.datetime.datetime(2012, 6, 12, 12)),
73           t_range[0], zorder=-10, facecolor='0.9',
74           edgecolor='none')
75 ax.text(0.13, 0.9, 'Mooring_falling\ntoward_seafloor',
76         ha='center', va='top', transform=ax.transAxes,
77         size='small')
78 ax.text(t_range[0] + 0.0001, 0.6, 'Mooring_on_seafloor',
79         size='small',
80         ha='left')
81 ax.annotate('', (t_range[0] + 0.006, 0.3),
82            (t_range[0], 0.3),
83            arrowprops=dict(facecolor='black', shrink=0.0),
84            ha='right')
85
86 # Finalize the figure
87 # Format the time axis:
88 tkr = dt.MinuteLocator(interval=5)
89 frmt = dt.DateFormatter('%H:%M')
90 ax.xaxis.set_major_locator(tkr)
91 ax.xaxis.set_minor_locator(dt.MinuteLocator(interval=1))
92 ax.xaxis.set_major_formatter(frmt)
93 ax.set_ylim([-3, 3])
94
95 # Label the axes:
96 ax.set_ylabel('$u$, \mathrm{[m/s]}$', size='large')
97 ax.set_xlabel('Time_[June_12,_2012]')
98 ax.set_title('Data_cropping_and_cleaning')

```

```

99 ax.set_xlim([dt.date2num(dt.datetime.datetime(2012, 6, 12, 12)),
100              dt.date2num(dt.datetime.datetime(2012, 6, 12, 12, 30))])
101
102 # Save the figure:
103 fig.savefig('./fig/crop_data.pdf')
104 # end cropping figure
105 #####
106
107 # Perform motion correction (including rotation into earth frame):
108 dat.props['body2head_vec'] = body2head_vec
109 dat.props['body2head_rotmat'] = body2head_rotmat
110 mc = adv.motion.CorrectMotion(accel_filter)
111 mc(dat)
112
113 ax.plot(dat.mpltime, dat.u, 'b-')
114
115 # Then rotate it into a 'principal axes frame':
116 adv.rotate.earth2principal(dat)
117 adv.rotate.earth2principal(dat_cln)
118
119 # Define an averaging object, and create an 'averaged' data set:
120 binner = adv.TurbBinner(n_bin=19200, fs=dat.fs, n_fft=4096)
121 dat_bin = binner(dat)
122 dat_cln_bin = binner(dat_cln)
123
124 # At any point you can save the data:
125 dat_bin.save('adv_data_rotated2principal.h5')
126
127 # And reload the data:
128 dat_bin_copy = adv.load('adv_data_rotated2principal.h5')
129
130 #####
131 # Figure to look at spectra
132 fig2 = plt.figure(2, figsize=[6, 6])
133 fig2.clf()
134 ax = fig2.add_axes([.14, .14, .8, .74])
135
136 ax.loglog(dat_bin.freq, dat_bin.Suu_hz.mean(0),
137           'b-', label='motion_corrected')
138 ax.loglog(dat_cln_bin.freq, dat_cln_bin.Suu_hz.mean(0),
139           'r-', label='no_motion_correction')
140
141 # Add some annotations
142 ax.axhline(1.7e-4, color='k', zorder=21)
143 ax.text(2e-3, 1.7e-4, 'Doppler_noise_level', va='bottom', ha='left',)
144
145 ax.text(1, 2e-2, 'Motion\nCorrection')
146 ax.annotate('', (3.6e-1, 3e-3), (1, 2e-2),
147            arrowprops={'arrowstyle': 'fancy',
148                       'connectionstyle': 'arc3,rad=0.2',
149                       'facecolor': '0.8',

```

```

150         'edgecolor': '0.6',
151     },
152     ha='center',
153 )
154
155 ax.annotate('', (1.6e-1, 7e-3), (1, 2e-2),
156             arrowprops={'arrowstyle': 'fancy',
157                         'connectionstyle': 'arc3,rad=0.2',
158                         'facecolor': '0.8',
159                         'edgecolor': '0.6',
160                         },
161             ha='center',
162 )
163
164 # Finalize the figure
165 ax.set_xlim([1e-3, 20])
166 ax.set_ylim([1e-4, 1])
167 ax.set_xlabel('frequency [hz]')
168 ax.set_ylabel('$\mathrm{[m^2s^{-2}/hz]}$', size='large')
169
170 f_tmp = np.logspace(-3, 1)
171 ax.plot(f_tmp, 4e-5 * f_tmp ** (-5. / 3), 'k--')
172
173 ax.set_title('Velocity_Spectra')
174 ax.legend()
175 #ax.axhspan(1e-4, 3e-4, facecolor='w', alpha=0.8, zorder=10, edgecolor='none')
176 ax.axvspan(1, 16, 0, .2, facecolor='0.8', zorder=-10, edgecolor='none')
177 ax.text(4, 4e-4, 'Doppler_noise', va='bottom', ha='center',
178        #bbox=dict(facecolor='w', alpha=0.9, edgecolor='none'),
179        zorder=20)
180
181 fig2.savefig('./fig/motion_vel_spec.pdf')

```

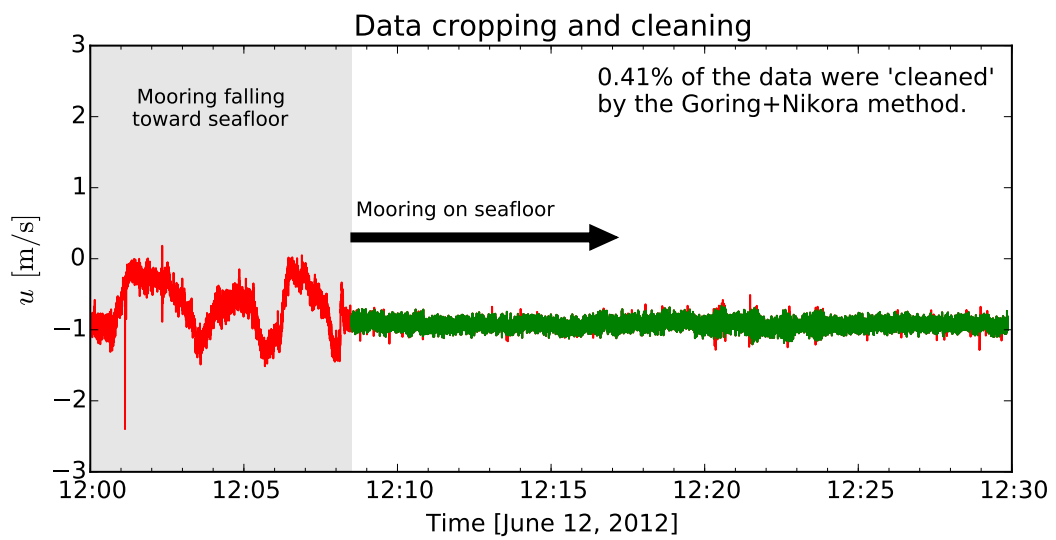


Figure 13. The 'crop_data.pdf' figure generated by the adv_example01.py script. The uncropped, uncleaned data is in red, and the cropped and cleaned data is in blue.

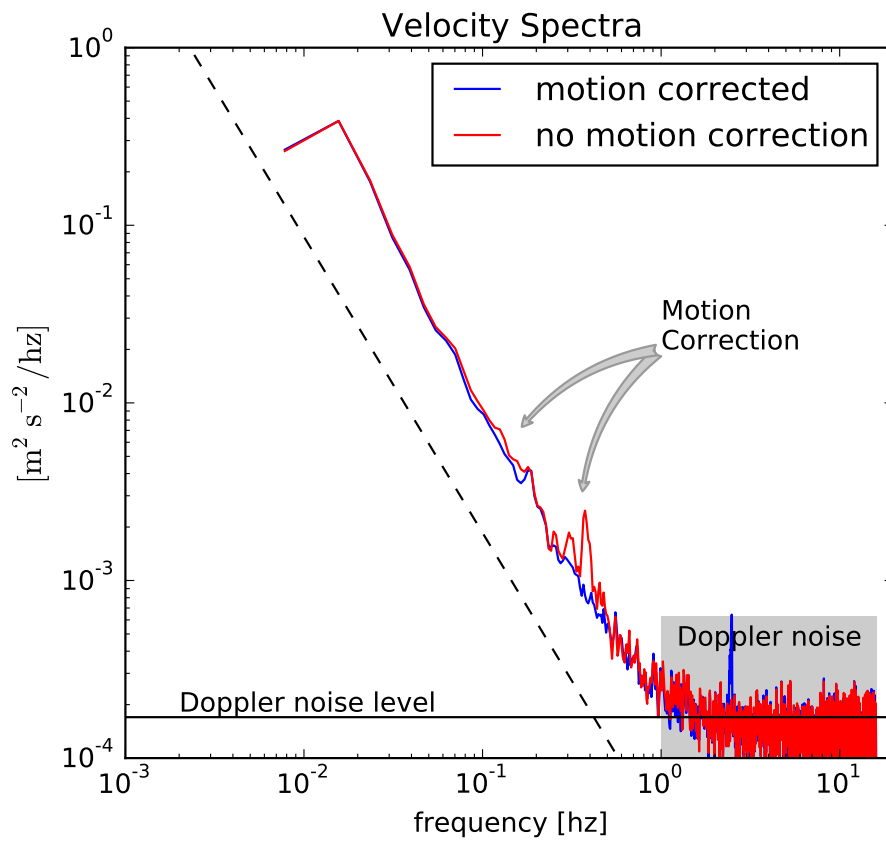


Figure 14. The 'motion_vel_spec.pdf' figure generated by the adv_example01.py script. Spikes in the spectra due to motion contamination (red) are removed by motion correction (blue).